Optimization of Time- and Code-Division-Multiplexed Readout for Athena X-IFU

W. Bertrand Doriese, Simon R. Bandler, Saptarshi Chaudhuri, Carl S. Dawson, Edward V. Denison, Shannon M. Duff, Malcolm Durkin, Connor T. FitzGerald, Joseph W. Fowler, Johnathon D. Gard, Gene C. Hilton, Kent D. Irwin, Young Il Joe, Kelsey M. Morgan, Galen C. O'Neil, Christine G. Pappas, Carl D. Reintsema, David A. Rudman, Stephen James Smith, Robert W. Stevens, Daniel S. Swetz, Paul Szypryt, Joel N. Ullom, Leila R. Vale, Joel C. Weber, and Betty A. Young

***Abstract*—Readout of a large, spacecraft-based array of superconducting transition-edge sensors (TESs) requires careful management of the layout area and power dissipation of the cryogenic-circuit components. We present three optimizations of our time- (TDM) and code-division-multiplexing (CDM) systems for the X-ray integral field unit (X-IFU), a several-thousand-pixel-TES array for the planned Athena-satellite mission. The first optimization is a new readout scheme that is a hybrid of CDM and TDM. This C/TDM architecture balances CDM's noise advantage with TDM's layout compactness. The second is a redesign of a component: the shunt resistor that provides a dc-voltage bias to the TESs. A new layout and a thicker Pd-Au resistive layer combine to reduce this resistor's area by more than a factor of 5. Third, we have studied the power dissipated by the first-stage superconducting quantum-interference devices (SQUIDs) and the readout noise versus the critical current of the first-stage SQUIDs. As a result, the X-IFU TDM and C/TDM SQUIDs will have a specified junction critical current of 5 μA. Based on these design optimizations and TDM experiments described by Durkin *et al.* (these proceedings), TDM meets all requirements to be X-IFU's backup-readout option. Hybrid C/TDM is another viable option that could save spacecraft resources.**

Manuscript received October 30, 2018; accepted March 9, 2019. Date of publication March 18, 2019; date of current version April 17, 2019. The authors gratefully acknowledge funding from the NASA SAT program "Providing Enabling & Enhancing Technologies for a Demonstration Model of the Athena X-IFU." *(Corresponding author: W. Bertrand Doriese.)*

W. B. Doriese, E. V. Denison, S. M. Duff, M. Durkin, J. W. Fowler, J. D. Gard, G. C. Hilton, Y. I. Joe, K. M. Morgan, G. C. O'Neil, C. G. Pappas, C. D. Reintsema, D. A. Rudman, R. W. Stevens, D. S. Swetz, P. Szypryt, J. N. Ullom, L. R. Vale, and J. C. Weber are with the National Institute of Standards and Technology, Boulder, CO 80305 USA (e-mail: doriese@boulder.nist.gov; carl.dawson@stanford.edu).

S. R. Bandler and S. J. Smith are with National Aeronautics and Space Administration, Greenbelt, MD 20771 USA (e-mail: simon.r.bandler@nasa.gov; stephen.j.smith@nasa.gov).

S. Chaudhuri, C. S. Dawson, and K. D. Irwin are with the Department of Physics, Stanford University, Stanford, CA 94305 USA (e-mail: schaudh2@stanford.edu; irwin@stanford.edu).

C. T. FitzGerald is with the Department of Physics, Santa Clara University, Santa Clara, CA 95053 USA (e-mail: cfitzgerald@scu.edu).

B. A. Young is with the Department of Physics, Stanford University, Stanford, CA 94305 USA, and also with the Department of Physics, Santa Clara University, Santa Clara, CA 95053 USA (e-mail: byoung@scu.edu).

Color versions of one or more of the figures in this paper are available online at http://ieeexplore.ieee.org.

Digital Object Identifier 10.1109/TASC.2019.2905577

***Index Terms*—Transition-edge sensors, superconducting quantum-interference devices, multiplexed readout, X-ray microcalorimeters, athena satellite.**

I. Introduction

THE X-ray Integral Field Unit (X-IFU) [1] is a 3,168 pixel imaging spectrometer of transition-edge sensors (TESs) planned for the European Space Agency's Athena X-ray observatory. Large arrays of cryogenic sensors require multiplexed readout to reduce the complexity, heat load, and wire count. Frequency-division multiplexing via megahertz ac bias of the TESs [2], [3] is the baseline readout technology for X-IFU. Schemes such as time-division-SQUID (superconducting quantum-interference device) multiplexing, or TDM [4], and code-division multiplexing (CDM) [5], in which the TESs are dc-biased, are backup-readout options.

Instrumentation for spacecraft is designed to minimize parameters like power, mass, and volume. Thus, although our TDM system is highly mature for terrestrial X-ray spectrometers [6] and has flown in space aboard the Micro-X sounding rocket [7] in July 2018, further development for X-IFU has been required. In this paper, we discuss three recent development areas. The first (Sec. II) is a new scheme that is a hybrid of TDM and code-division multiplexing (CDM) [5], which we denote C/TDM. The next (Sec. III) is to make the TES-shunt resistors more compact. The third (Sec. IV) is to optimize the critical current of the first-stage SQUIDs to obtain acceptable noise while remaining within the power budget.

Recent 40-row TDM experiments [8] with X-IFU-like TESs [9] used the new shunt resistors and the optimized first-stage SQUIDs described here. The achieved 40-row energy resolution was (1.91 $\pm$ 0.01) eV at 1.5 keV, (2.23 $\pm$ 0.02) eV at 5.9 keV, (2.40 $\pm$ 0.02) eV at 6.9 keV, and (3.44 $\pm$ 0.04) eV at 11.9 keV; these results are compliant with the X-IFU energy-resolution budget. With the improvements described here, TDM and C/TDM are also compliant with the spacecraft envelope for Athena X-IFU.

U.S. Government work not protected by U.S. copyright.

Authorized licensed use limited to: NIST Virtual Library (NVL). Downloaded on June 23,2020 at 15:39:31 UTC from IEEE Xplore. Restrictions apply.

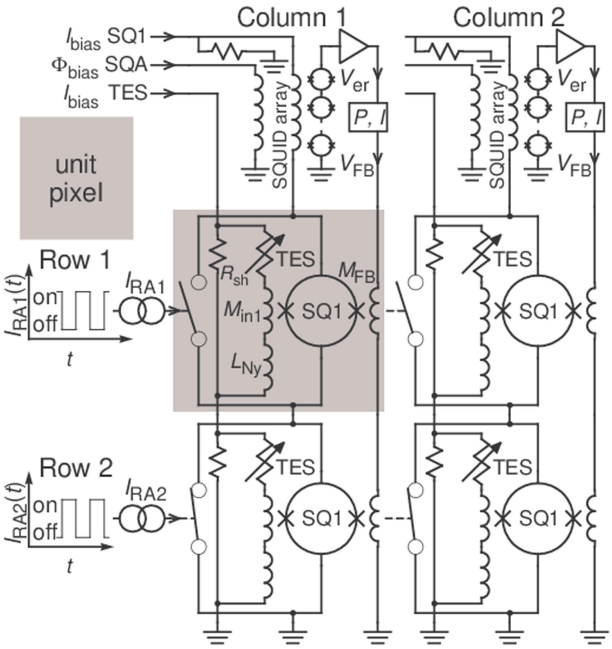

Fig. 1. Representative schematic of a 2-column × 2-row TDM. Each dc-biased TES is inductively coupled (M_{in1}) to its own first-stage SQUID amplifier (SQ1). Rows of SQ1s are sequentially turned on via application of a row-address current (I_{RA}) to their flux-actuated switches. The signal from one TES at a time per column is passed to that column's SQUID-series-array amplifier, whose voltage is then amplified by a high-bandwidth, room-temperature amplifier. To keep the non-linear, two-stage SQUID amplifier in a small, linear range, each column is run as a digitally interleaved flux-locked loop. The column's output voltage, or error signal (V_{er}), is digitally sampled, and then a proportional-integral flux-feedback signal (V_{FB}) is applied inductively (M_{FB}) to the SQ1s to servo V_{er} to a constant value. A linear combination of V_{FB} and V_{er} estimates the TES current.

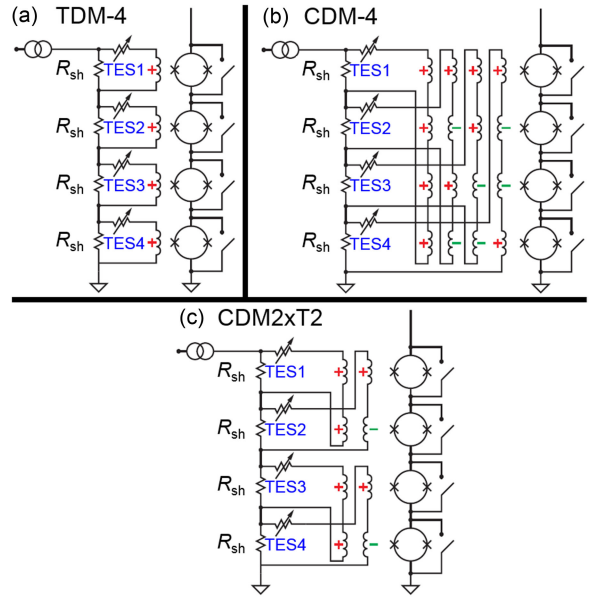

Fig. 2. 1-column × 4-row schematics of TDM, CDM, and C/TDM. (a) 4-row TDM. (b) Φ-CDM. (c) Hybrid: 2-row flux-summing CDM in time division with another 2-row flux-summing CDM, or CDM2xT2. In all three of these examples, the SQ1s are run as 4-row TDM. Only the TES couplings are different. An option for X-IFU is CDM16xT4, or four TDM'ed banks each of 16-row CDM.

II. TDM, CDM, AND C/TDM FOR X-IFU

A. TDM for X-IFU

In TDM readout, the TESs are dc-biased, each TES is coupled to its own first-stage SQUID (SQ1), rows of SQ1s are switched on one at a time, and columns of SQUIDs are read out in parallel. The TDM architecture proposed as the backup option for X-IFU is summarized in Fig. 1. It is further described in the literature [4].

B. CDM for X-IFU

In standard CDM, TES signals are multiplexed via modulation of their readout polarities between positive and negative. The basis set in N-row CDM is a *Walsh matrix* [10], W_{N}, and has N orthogonal rows whose entries are +1 and –1. Fig. 2b shows a W_4 matrix implemented via the technique of flux-summing CDM (Φ-CDM) [12]. As in TDM, the TESs are dc-biased. The SQ1s are run as a TDM. However, within a Φ-CDM block, each TES is coupled to all SQ1s; the Walsh matrix is encoded in the polarity of the input couplings.

The reason to use this more complicated scheme is that it results in lower multiplexed readout noise. CDM uses its readout bandwidth more efficiently than TDM because all TESs are sampled during each row period. Thus, CDM does not suffer TDM's $\sqrt{N_{\mathrm{rows}}}$ aliasing of readout noise [5], [11]. CDM is under consideration for X-IFU because it allows a higher multiplexing factor of 64 rows with lower readout noise than 40-row TDM. Our present version of TDM does not have the required combination of noise and dynamic range to meet X-IFU's requirements with a multiplexing factor of 64. A higher multiplexing factor in turn yields significant reductions in the power, mass, and volume of X-IFU's room-temperature readout electronics.

Analysis of 64-row Φ-CDM for X-IFU has uncovered two drawbacks. The first is that the layout area needed to coil-couple each block of 64 TESs to each block of 64 SQ1s does not fit within the design envelope of the X-IFU focal-plane assembly. The area per pixel scales roughly as the square of the Φ-CDM factor. The second issue is the potential for low fabrication yield in 64-row Φ-CDM coil couplers. The total number of wire crossovers scales as between the square and the cube of the Φ-CDM factor. Each wire crossover carries the small probability of a short circuit. We have fabricated and tested 32-row Φ-CDM chips [5]. Based on extrapolation of yield statistics of these chips, 64-row Φ-CDM was deemed too risky for X-IFU. This analysis led us to look for an alternative to 64-row Φ-CDM.

C. C/TDM for X-IFU

Our new technique, a hybrid of TDM and CDM, maintains enough of CDM's noise advantage to allow 64-row multiplexing within a circuit that is fabricable. In C/TDM, blocks of CDM are embedded in a larger TDM column. Each TES couples to more than one SQ1, but not to all SQ1s within a column. Fig. 2 shows three ways to read out four TESs in one column: standard 4-row TDM (TDM-4), standard 4-row CDM (CDM-4), and the hybrid scheme of 2-row CDM with a TDM factor of 2, which we call CDM2 × T2. For X-IFU, we propose 16-row CDM with a TDM factor of 4, or CDM16 × T4.

When the TES current changes rapidly, as during the onset of an X-ray pulse, the flux-locked loop (FLL) of any SQ1 row

Authorized licensed use limited to: NIST Virtual Library (NVL). Downloaded on June 23,2020 at 15:39:31 UTC from IEEE Xplore. Restrictions apply.

to which that TES is connected is driven away from its stable lockpoint and must recover. The FLL measures the error signal, computes the feedback flux needed to bring the error signal back to zero, and then applies that feedback flux when the SQ1 row is next addressed (during the next readout frame). The FLL remains locked if the error flux accumulated within a frame,

$$\Delta\Phi = (\mathrm{d}I/\mathrm{d}t)\, M_{\mathrm{in}} N_{\mathrm{rows}} t_{\mathrm{row}}, \tag{1}$$

fits within the usable linear flux range of the SQ1. Here, dI/dt is the current slew-rate, $N_{\mathrm{rows}} = 64$ is the total CDM$*$TDM multiplexing factor, and $t_{\mathrm{row}} = 160$ ns is the row period. When our modern flux-actuated SQ1 [4] is operated on its steep slope, where the ratio of the linear flux range to the noise [14] is best, the usable linear flux range is 0.30 Φ_0. Because in CDM each SQ1 sees both positive and negative flux pulses, the SQ1 is locked in the center of its modulation depth; a TES-current pulse is thus allowed a maximum flux excursion of half the linear range, or 0.15 Φ_0. The maximum X-ray energy of interest to X-IFU is 12 keV. Under the circuit and bias conditions used in the 40-row readout experiments [8], the maximum current slew-rate from a 12 keV X-ray, averaged across the array, was 0.262 A/s. For X-IFU, we budget $(\mathrm{d}I/\mathrm{d}t)|_{\max} = 0.280$ A/s to allow some variation among pixels. Solving Eq. 1 for M_{in} gives $M_{\mathrm{in}} \leq 108$ pH. To allow an additional 10% margin in slew rate, we choose $M_{\mathrm{in}} = 98$ pH.

In a C/TDM system, the multiplexed, TES-referred noise is given by:

$$\sqrt{S_{I_{\mathrm{MUX}}}} = \frac{\sqrt{\pi N_{\mathrm{TDM}} S_{\Phi}}}{M_{\mathrm{in1}}}, \tag{2}$$

where $N_{\mathrm{TDM}} = 4$ is the TDM factor. At the targeted, non-multiplexed readout-noise level of $\sqrt{S_{\Phi}} = 0.20\,\mu\Phi_0/\sqrt{\mathrm{Hz}}$, which was achieved in a previous generation of SQ1s [4] of design similar to that proposed for X-IFU, the TESs will see multiplexed readout noise of 14.9 pA/$\sqrt{\mathrm{Hz}}$. This is about 10% lower than the equivalent 40-row TDM readout-noise level and about half the maximum of 29.7 pA/$\sqrt{\mathrm{Hz}}$ allowed by the X-IFU energy-resolution budget to achieve $\Delta E = 2.5$ eV at 7 keV. Thus, CDM16 $\times$ T4 allows a multiplexing factor of 64 within X-IFU's performance specifications.

Multiplexer chips containing individual blocks of 16-row CDM were fabricated and have been verified in a 4 K dip probe [13] to have basic functionality. Testing of the full CDM16 $\times$ T4 scheme with TESs will occur in a new 960-pixel readout platform that is presently under development.

III. TES Shunt Resistors for X-IFU

In TDM and C/TDM readout, the TESs are dc-biased. A dc-current bias is applied to the TES-bias loop (see Fig. 1); a shunt resistor, R_{shunt}, whose resistance is much smaller than the TES operating resistance, R_{TESop}, generates a voltage bias across the TES. Lower R_{shunt} yields a harder voltage bias, which generally leads to both better inherent TES energy resolution and increased immunity to fluctuations in the thermal and magnetic environments. The TDM/CDM X-IFU-like TESs [9] use $R_{\mathrm{TESop}} \sim 1$ mΩ. The targeted value of R_{shunt} is 75 $\mu\Omega$. Our previous

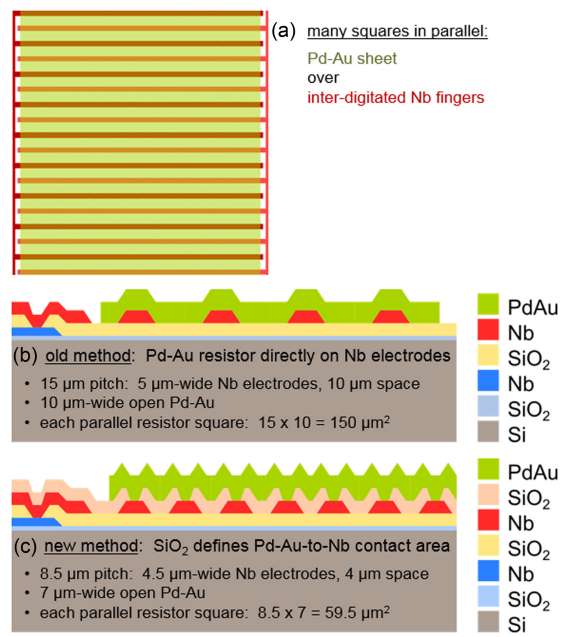

Fig. 3. TES-shunt resistors. (a) The very low resistance value requires many squares of a Pd-Au sheet to be wired in parallel. The Pd-Au (target is 53% Pd: 47% Au by mass) [15] is laid over a pair of superconducting electrodes of interdigitated Nb. (b) Cross-sectional diagram of the old method of fabrication in which the Pd-Au contacted the Nb directly. This design's component area was prohibitive for X-IFU. (c) Cross-sectional diagram of the new method of fabrication in which an insulating layer separates the Pd-Au from the Nb except at defined openings. This design allows much more compact resistors.

lab-based spectrometers [6], which did not have X-IFU's stringent performance requirements, have typically used $R_{\mathrm{shunt}} \sim 300\ \mu\Omega$ to 400 $\mu\Omega$ with $R_{\mathrm{TESop}} \sim 1$ mΩ.

Alloyed resistive materials at practical thicknesses offer $R_{\mathrm{sheet}} \sim 1\ \Omega$/square in the 55 mK temperature range; thus, a very short and wide resistive sheet is required to reach $R_{\mathrm{shunt}} = 75\ \mu\Omega$. In our design (Fig. 3a), the superconducting Nb electrodes are inter-digitated fingers. Pd-Au is overlaid to create many resistive squares in parallel. Without a re-design of our standard TES-shunt resistors, their surface area would have been a design driver for TDM and C/TDM readout in X-IFU.

In our old design (Fig. 3b), the Pd-Au resistive sheet is laid directly on the Nb electrodes. To minimize the effects of lateral proximitization of the Pd-Au resistor by the Nb superconductor and vice versa, the 5 μm width and 10 μm spacing of the Nb fingers are both much larger than the practical size limits of the lithography and etching techniques used to create them. Lateral proximitization could cause either or both of the following undesirable behaviors: dependence of R_{shunt} on I_{bias}; and differences among fabrication runs in R_{shunt} due to run-to-run variation in the Pd-Au-to-Nb contact interfaces on the sloped side walls of the Nb. This design requires a component area per parallel square of $A_{\mathrm{square}} = 150\ \mu\mathrm{m}^2$. Our standard 225 nm-thick Pd-Au yields 1.2 Ω/square at 55 mK, so a 75 $\mu\Omega$ shunt resistor requires an area of 1.8 mm^2.

In our new design, an extra SiO_2 insulating layer separates the Pd-Au resistor from the Nb electrodes. Open slits in the SiO_2 of width 1.5 μm allow the Pd-Au to contact only on the tops of the Nb fingers. Sidewall interfaces are thus eliminated. Here, the Nb width is reduced slightly to 4.5 μm and the finger

Authorized licensed use limited to: NIST Virtual Library (NVL). Downloaded on June 23,2020 at 15:39:31 UTC from IEEE Xplore. Restrictions apply.

spacing is reduced a lot to 4 μm. The width of the open Pd-Au between finger contacts is 7 μm. This design requires component area per parallel square of $A_{\rm square} = 59.5\ \mu{\rm m}^2$. Thicker, 470 nm Pd-Au yields 0.574 Ω/square at 55 mK, so a 75 $\mu\Omega$ shunt resistor requires area of 0.34 mm^2. Areal density is 5.3 times that of the old design. Shunt resistors of this new design fit comfortably within the design envelope of the X-IFU focal-plane assembly. Resistors of this new design have been fabricated and were used successfully in the recent 40-row TDM experiments [8].

IV. SQUID Power and Noise Versus Critical Current

The 55 mK stage of the X-IFU is cooled by an adiabatic demagnetization refrigerator with a planned total cooling power on order 1 μW. This cooling power is allocated among many sub-systems. In the TDM and C/TDM cryogenic-power budgets for X-IFU, the SQ1s are allocated a total of on order tens of nanowatts. One SQ1 at a time is turned on per column. Depending on the multiplexing factor, which is still under discussion, each TDM or C/TDM readout column is permitted a nominal power budget of roughly 450 pW for its SQ1s. Here we present the results of a study of TDM-readout noise vs. SQ1 power.

The maximum SQUID critical current, $I_{\rm C}$, is a tunable fabrication parameter that affects both noise and power. A SQ1 with a higher $I_{\rm C}$ will have a somewhat taller *I*-vs.-Φ curve; this higher gain lowers the quadrature contributions of all downstream noise sources, such as the series-array-SQUID amplifier and room-temperature amplifier (see Fig. 1), so the overall readout noise will be lower. It will also dissipate more power on the 55 mK stage. In our study, TDM chips of the same lithographic design, "mux18b," were produced on two wafers whose Nb/Al-Al_2O_3/Nb tri-layers [16] were fabricated to attain different critical currents. One wafer had $I_{\rm C} = 10.6\ \mu$A (junction critical current of 5.3 μA). The other had $I_{\rm C} = 15.0\ \mu$A (junction critical current of 7.5 μA). This range of critical currents spans the range of our typical devices.

Fig. 4 shows the (a) *I*-vs.-Φ and (b) power-vs.-Φ curves for representative SQ1s from the two wafers at two bias points each: 110% and 140% of their respective critical currents. As predicted, the 15 μA SQ1 has a taller *I*-vs.-Φ curve and its power dissipation is proportionally larger. At the highest combination (dashed-red line) of critical current (15 μA) and bias (140%), the power at the center of the modulation depth is right at the targeted 450 pW. The typical quiescent lockpoint is near the bottom of the modulation depth, so even the highest-power SQ1 curve shown here is compliant with the 450 pW budget.

The recent 40-row TDM experiments [8] used one column of 10.6 μA mux18b chips and two columns of 15.0 μA mux18b chips. The average SQ1 bias was about 125% of $I_{\rm C}$. The average, TES-referred, 40-row TDM-readout noise in the 10.6 μA column was 25.6 pA/$\sqrt{\rm Hz}$, which translates [11] to a non-multiplexed, SQ1-referred value of $\sqrt{S_\Phi} = 0.31\,\mu\Phi_0/\sqrt{\rm Hz}$. Across the two 15.0 μA columns, these values averaged 23.4 pA/$\sqrt{\rm Hz}$ and $\sqrt{S_\Phi} = 0.31\,\mu\Phi_0/\sqrt{\rm Hz}$, respectively. Both values are below the 29.7 pA/$\sqrt{\rm Hz}$ allowed by the X-IFU energy-resolution budget. However, both values are significantly above the X-IFU 40-row TDM target of 16.7 pA/$\sqrt{\rm Hz}$. The target is based on non-multiplexed, SQ1-referred noise of

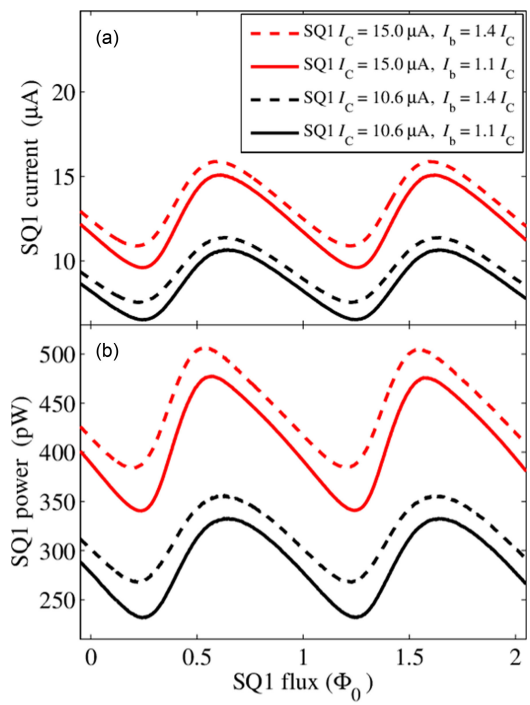

Fig. 4. Modulation curves for SQ1s of two different critical currents and under two different bias conditions. (a) SQ1 current vs. flux. (b) SQ1 power vs. flux. At the highest combination (dashed-red line) of critical current (15 μA) and bias (140%), the power at the center of the modulation depth is 450 pW.

$0.20\,\mu\Phi_0/\sqrt{\rm Hz}$; this performance was previously achieved [4] with 10 μA SQ1s that differ from the present mux18b's only in the strength of their input coupling, $M_{\rm in}$. We continue to investigate why the mux18b SQ1s did not reach the targeted noise level.

V. Conclusion

We have studied several areas of our mature time-division-multiplexing architecture to assure compliance with the various budgets of Athena X-IFU. Recent 40-row-TDM experiments [8] with X-IFU-like TESs verified the readout performance and energy resolution. We have improved the areal density of our TES-shunt resistors by more than a factor of 5 to assure a fit within the volume budget of the focal-plane assembly. We have tested first-stage SQUIDs of different critical currents and verified that the devices meet the required noise specifications and are within the power budget. Thus, our TDM design is well suited to be the backup readout option for X-IFU. In addition, we continue to develop code-division multiplexing for X-IFU as an option that could save additional spacecraft resources while still meeting the performance requirements.

Acknowledgment

The X-IFU's international "Time-Division-Multiplexing Working Group" (2017–2018) undertook a thorough analysis of TDM and C/TDM for X-IFU. The authors thank the group members from CNES, IRAP, APC, SRON, NASA, Stanford, and NIST for many helpful technical discussions. The authors gratefully acknowledge funding from the NASA SAT program "Providing Enabling & Enhancing Technologies for a Demonstration Model of the Athena X-IFU."

Authorized licensed use limited to: NIST Virtual Library (NVL). Downloaded on June 23,2020 at 15:39:31 UTC from IEEE Xplore. Restrictions apply.

REFERENCES

[1] D. Barret *et al.*, "The ATHENA X-ray integral field unit (X-IFU)," in *Proc. SPIE– Int. Soc. Opt. Eng.*, vol. 10699. Austin, TX, USA, 2018, Art. no. 106991G.

[2] J. van der Kuur *et al.*, "Optimising the multiplex factor of the frequency domain multiplexed readout of the TES-based microcalorimeter imaging array for the X-IFU instrument on the Athena x-ray observatory," *Proc. SPIE Astron. Telescopes + Instrum.*, vol. 9905. Edinburgh, U.K., 2016, Art. no. 99055R.

[3] H. Akamatsu *et al.*, "Development of frequency domain multiplexing for the X-ray Integral Field unit (X-IFU) on the Athena," *Proc. SPIE Astron. Telescopes + Instrum.*, vol. 9905. Edinburgh, U.K., 2016, Art. no. 99055S.

[4] W. B. Doriese *et al.*, "Developments in time-division multiplexing of x-ray transition-edge sensors," *J. Low Temp. Phys.*, vol. 184, pp. 389–395, 2016.

[5] K. M. Morgan *et al.*, "Code-division-multiplexed readout of large arrays of TES microcalorimeters," *Appl. Phys. Lett.*, vol. 109, 2016, Art. no. 112604.

[6] W. B. Doriese *et al.*, "A practical superconducting-microcalorimeter X-ray spectrometer for beamline and laboratory science," *Rev. Sci. Instrum.*, vol. 88, 2017, Art. no. 053108.

[7] D. C. Goldfinger *et al.*, "Detector calibration for the micro-X sounding rocket -ray telescope," *J. Low Temp. Phys.*, vol. 193, pp. 984–990, 2018, [Online]. Available: https://doi.org/10.1007/s10909-018-2060-7.

[8] M. Durkin *et al.*, "Demonstration of Athena-X-IFU-compatible 40-row time-division-multiplexed readout," *IEEE Trans. Appl. Supercond.*, to be published, doi: 10.1109/TASC.2019.2904472.

[9] A. R. Miniussi *et al.*, "Performance of an X-ray microcalorimeter with a 240 μm absorber and a 50 μm TES bilayer," *J. Low Temp. Phys.*, vol. 193, pp. 337–343, 2018, [Online]. Available: https://doi.org/10.1007/s10909-018-1974-4.

[10] K. G. Beauchamp, *Walsh Functions and their Applications*. London, U.K.: Academic Press, 1975.

[11] W.B. Doriese *et al.*, "Progress toward kilopixel arrays: 3.8 eV microcalorimeter resolution in 8-channel SQUID multiplexer," *Nucl. Instrum. Methods Phys. Res. Sect. A*, vol. 559, pp. 808–810, 2006.

[12] G. M. Stiehl *et al.*, "Code-division multiplexing for x-ray microcalorimeters," *Appl. Phys. Lett.*, vol. 100, 2012, Art. no. 072601.

[13] C. D. Reintsema *et al.*, "A methodology for high-throughput DC parametric evaluation of flux activated switch based TDM and CDM SQUID multiplexers," presented at the Appl. Supercond. Conf., Seattle, WA, USA, Oct. 28–Nov. 2, 2018, doi: 10.1109/TASC.2019.2904594.

[14] W. B. Doriese *et al.*, "Optimization of the TES-Bias circuit for a multiplexed microcalorimeter array," *J. Low Temp. Phys.*, vol. 167, pp. 595–601, 2012.

[15] C. Y. Ho *et al.*, "Electrical resistivity of ten selected binary alloy systems," *J. Phys. Chem. Ref. Data*, vol. 12, pp. 183–322, 1983.

[16] J. E. Sauvageau, C. J. Burroughs, P. A. A. Booi, M. W. Cromar, R. P. Benz, and J. A. Koch, "Superconducting integrated circuit fabrication with low temperature ECR-based PECVD SiO_2 dielectric films," *IEEE Trans. Appl. Supercond.*, vol. 5, no. 2, pp. 2303–2309, Jun. 1995.

Authorized licensed use limited to: NIST Virtual Library (NVL). Downloaded on June 23,2020 at 15:39:31 UTC from IEEE Xplore. Restrictions apply.